Transient Field-Circuit Coupled Models with Switching Elements for the Simulation of Electric Energy Transducers*

Herbert De Gersem, Galina Benderskaya, and Thomas Weiland

Technische Universität Darmstadt, Institut für Theorie Elektromagnetischer Felder,
Schloßgartenstraße 8, D-64289 Darmstadt, Germany
DeGersem@temf.tu-darmstadt.de

This paper deals with the transient simulation of large, nonlinear magnetoquasistatic field models which are monolithically coupled to electric circuits. Solid- and stranded-conductor models embedded in the field model are connected to the external circuit. In order to guarantee the numerical efficiency of the field-circuit coupled formulation, conductor models coupling the circuit to the field at a reference cross-section, have to be preferred over conductor models that couple the whole conductor volume to the circuit. The circuit is formulated in terms of both voltage drops and currents in order to avoid fill-in in the field matrix parts. For time stepping, an error-controlled, adaptive singly diagonally Runge-Kutta method is applied. A dense output solution is used to detect and localise switching events in the circuit. The actual time step is restricted to the time instant of switching at which consistent initial conditions are determined before restarting the time integration. The transient field-circuit coupling is applied to the models of a capacitor motor and a three-phase transformer.

1 Introduction

Contemporary designs of electrical-energy convertors force the machine to operate at higher flux densities and higher frequencies, leading to higher levels of ferromagnetic saturation and eddy currents, respectively. Two- and three-dimensional field simulation are indispensable to resolve these kinds of local effects. However, the power-electronic components connected to the device and, in the two-dimensional case, the interconnections between the different conductors, are commonly excluded from the field model. To uniquely define the field model, the voltage drops along the massive conductors and the currents through the coils have to be known a-priori, which is impractical. The interaction of the device with external excitation and load circuits can be very complicated such that engineers are obliged to iterate between the field and the circuit model, an approach which is called *simulator coupling*. Simulator coupling especially performs well when the time constants considered by both simulators are different by orders of magnitude. For situations where this is not the

* Invited Paper at SCEE-2006

case, a *monolithic coupling*, i.e., combining both the field and the circuit model into a single system of equations, is recommended. Monolithic coupling is especially valuable for coupling electromagnetic field and circuit simulation because the coupling itself is linear and can therefore be adequately represented at the algebraic level. Monolithic coupling requires, however, all stages of the coupling process to be designed carefully. A bad coupling approach and implementation leads to systems of equations that cause difficulties at the algebraic level, which may cause the performance of the monolithic coupling to be degenerated to the one of a simulator coupling.
The paper exemplarily describes the coupling of an electric circuit to a magnetoquasistatic field model. Couplings in other physical disciplines can be developed similarly. The field model is discretised by the finite-element method or the finite-integration technique. The coupling is designed from the field point-of-view, adding a few circuit equation to a large system of field equations, without too much influencing typical field simulation techniques to loose their performance. Hence, the approach is complementary to coupling procedures where field-simulation actions are embedded in an established circuit simulator.

2 Discrete Magnetoquasistatic Formulation

The magnetic flux density $\mathbf{B}$ is forced to be divergence-free by stating $\mathbf{B} = \nabla \times \mathbf{A}$ with $\mathbf{A}$ the magnetic vector potential. The integration of the Faraday-Lenz law yields the electric field strength $\mathbf{E} = -\frac{\partial}{\partial t}\mathbf{A} - \nabla\phi$ with the gradient of the electric scalar potential ϕ as an integration constant. The material properties are expressed in their easiest form. $\mathbf{B}$ is related to the magnetic field strength $\mathbf{H}$ by the reluctivity ν, i.e., $\mathbf{H} = \nu\mathbf{B}$ where ν may depend on $\mathbf{B}$. The current density $\mathbf{J}$ is related to $\mathbf{E}$ by the conductivity σ, i.e., $\mathbf{J} = \sigma\mathbf{E}$. The combination of the material laws and the potentials within Ampères law directly leads to the magnetoquasistatic formulation

$$\nabla \times (\nu\nabla \times \mathbf{A}) + \sigma\frac{\partial \mathbf{A}}{\partial t} = -\sigma\nabla\phi \; . \tag{1}$$

The righthandside is called the source current density $\mathbf{J}_\mathrm{s} = -\sigma\nabla\phi$.
In the case of the finite-integration technique (FIT), (1) is transferred to a staggered grid pair $(G, \tilde{G})$ [35, 36]. Here, only the special case of a structured, orthogonal grid pair is considered. The degrees of freedom are the magnetic vector potentials integrated along the edges L_i of the primary grid G, collected into the algebraic vector $\widehat{\mathbf{a}}$, i.e.,

$$\widehat{\mathbf{a}}_i = \int_{L_i} \mathbf{A} \cdot \mathrm{d}\mathbf{s} \; . \tag{2}$$

The application of the primary curl operator $\mathbf{C}$ gives $\widehat{\widehat{\mathbf{b}}} = \mathbf{C}\widehat{\mathbf{a}}$ where the components of $\widehat{\widehat{\mathbf{b}}}$ are the magnetic fluxes through the primary facets S_p. The magnetic material law is expressed at the crossing points between primary facets and dual edges. The magnetic voltage $\widehat{\mathbf{h}}_p$ along a dual edge $\tilde{L}_p$ reads

$$\widehat{\mathbf{h}}_p = \int_{\tilde{L}_p} \mathbf{H} \cdot \mathrm{d}\mathbf{s} \approx \mathbf{M}_{\nu,p,p}\widehat{\widehat{\mathbf{b}}}_p = \frac{\nu|\tilde{L}_p|}{|S_p|} \tag{3}$$

where the entries $\mathbf{M}_{\nu,p,p}$ are gathered in the diagonal *reluctivity matrix* $\mathbf{M}_\nu$. Similarly, the current $\widehat{\tilde{\mathbf{j}}}_q$ through a dual facet $\tilde{S}_q$ is related to the electric voltage $\widehat{\mathbf{e}}_q$ allocated at the associated primary edge by

$$\widehat{\tilde{\mathbf{j}}}_q = \int_{\tilde{S}_q} \mathbf{J} \cdot \mathrm{d}\mathbf{S} \approx \mathbf{M}_{\sigma,q,q} \widehat{\mathbf{e}}_q = \frac{\sigma |\tilde{S}_q|}{|L_q|} \tag{4}$$

with the *conductivity matrix* $\mathbf{M}_\sigma$. The discrete equivalent of Ampères law reads $\widehat{\tilde{\mathbf{j}}} = \widetilde{\mathbf{C}} \widehat{\mathbf{h}}$ where $\widetilde{\mathbf{C}}$ is the discrete curl operator at the dual grid. The operators $\mathbf{C}$ and $\widetilde{\mathbf{C}}$ do not incorporate any discretisation . The discretisation error is solely attributed to the material matrices $\mathbf{M}_\nu$ and $\mathbf{M}_\sigma$. The discrete counterpart of (1) reads

$$\widetilde{\mathbf{C}} \mathbf{M}_\nu \mathbf{C} \bar{\mathbf{a}} + \mathbf{M}_\sigma \frac{d\bar{\mathbf{a}}}{dt} = \widehat{\tilde{\mathbf{j}}}_\mathrm{s} \tag{5}$$

with $\widehat{\tilde{\mathbf{j}}}_\mathrm{s}$ the vector of the discrete source currents [7].
In the case of the finite-element (FE) method, the magnetic vector potential is expressed as a linear combination of n_fe edge elements $\mathbf{w}_j$. The FE formulation follows from weighting (1) by the test functions $\mathbf{w}_i$ and integrating by parts. The introduction of the discrete curl operators $\mathbf{C}$ and $\widetilde{\mathbf{C}}$ to the FE grid leads to the same formulation as (5) but with slightly different material matrices and source currents, here indicated by a superscript $\cdot^{(\mathrm{fe})}$:

$$\mathbf{M}^{(\mathrm{fe})}_{\nu,p,q} = \int_\Omega \nu \mathbf{z}_p \cdot \mathbf{z}_q \, \mathrm{d}\Omega \; ; \tag{6}$$

$$\mathbf{M}^{(\mathrm{fe})}_{\sigma,i,j} = \int_\Omega \sigma \mathbf{w}_i \cdot \mathbf{w}_j \, \mathrm{d}\Omega \; ; \tag{7}$$

$$\widehat{\tilde{\mathbf{j}}}^{(\mathrm{fe})}_{\mathrm{s,i}} = \int_\Omega (-\sigma \nabla \phi) \cdot \mathbf{w}_i \, \mathrm{d}\Omega \tag{8}$$

where Ω denotes the computational domain and $\mathbf{z}_p$ is the facet element associated with the primary grid facet S_p. In the following, a distinction between FIT and FE formulations is only made when absolutely necessary.

3 Conductor Models

3.1 Solid-conductor model

A massive conductor which covers the volume $\Omega_{\mathrm{sol},q}$ is excited by a voltage drop $u_{\mathrm{sol},q}$ between two electrodes (Fig. 1a). From the application of the Faraday-Lenz law along a closed contour passing along the massive conductor and through the voltage source, one finds that

$$u_{\mathrm{sol},q} = -\int_{\ell_{\mathrm{sol},q}} \nabla \phi \cdot \mathrm{d}\mathbf{s} \tag{9}$$

with $\ell_{\mathrm{sol},q}$ an arbitrary path between both electrodes. The potentials $\mathbf{A}$ and ϕ are, however, not unique, i.e., when $(\mathbf{A}, \phi)$ solves (1), so does $\left(\mathbf{A} + \psi, \phi + \frac{\partial}{\partial t}\psi\right)$ where

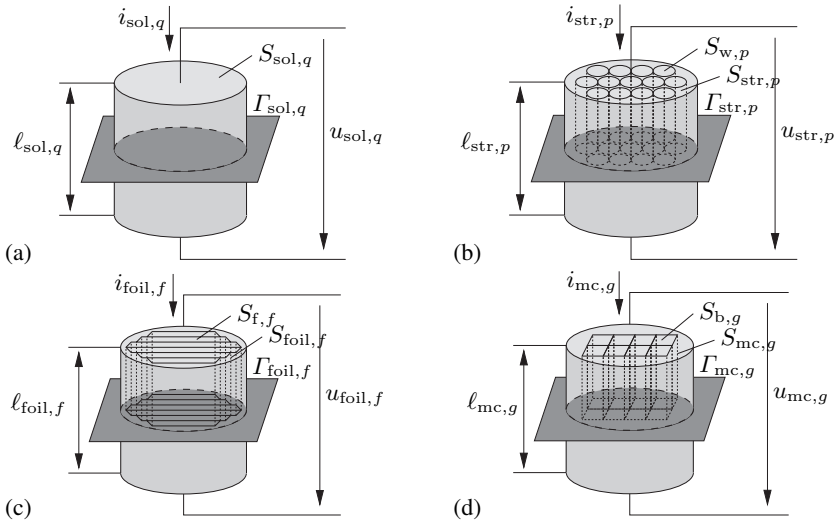

Fig. 1: (a) Solid-conductor model, (b) stranded-conductor model, (c) foil-conductor model and (d) multi-conductor model.

ψ is an arbitrary scalar field. As a consequence, the division of $\mathbf{J}$ into a *source-current density* $\mathbf{J}_{\mathrm{s}} = -\sigma\nabla\phi$ and an *eddy-current density* $\mathbf{J}_{\mathrm{e}} = -\sigma\frac{\partial}{\partial t}\mathbf{A}$ is not unique as well. Commonly, the formulation is closed by forcing the source-current density and the eddy-current density to be divergence-free. Then, the source-current density $\mathbf{J}_{\mathrm{s}} = -\sigma\nabla\phi_{\mathrm{s}}$ is obtained by solving the stationary-current problem $-\nabla\cdot(\sigma\nabla\phi_{\mathrm{s}}) = 0$ with the boundary conditions $\phi_{\mathrm{s}} = \phi_1$ and $\phi_{\mathrm{s}} = \phi_2$ at the electrodes such that $u_{\mathrm{sol},q} = \phi_2 - \phi_1$. The discrete equivalent reads

$$\widetilde{\mathbf{S}}\mathbf{M}_\sigma\widetilde{\mathbf{S}}^T\Phi_{\mathrm{s}} = 0 \tag{10}$$

where $\widetilde{\mathbf{S}}$ is the discrete divergence operator at the dual grid, $-\widetilde{\mathbf{S}}^T$ equals the discrete gradient operator at the primary grid and Φ_{s} is the vector of electrical scalar potentials allocated at the primary nodes. A particular field-circuit coupling scheme consists of solving (10) where a unit voltage drop between the electrodes is applied as a boundary condition. The resulting discrete source-current distribution is $\mathbf{M}_\sigma\mathbf{Q}_{\mathrm{sol},q} = \mathbf{M}_\sigma\widetilde{\mathbf{S}}^T\Phi_{\mathrm{s}}$ and defines a coupling operator $\mathbf{Q}_{\mathrm{sol},q}$ which allows to express the discrete source current generated by an arbitrary voltage drop $u_{\mathrm{sol},q}$ across the massive conductor q by $\widehat{\mathbf{j}}_{\mathrm{s}} = \mathbf{M}_\sigma\mathbf{Q}_{\mathrm{sol},q}u_{\mathrm{sol},q}$. The column vector $\mathbf{Q}_{\mathrm{sol},q}$ contain nonzero contributions for all primary edges in the massive-conductor volume. Hence, it represents a 3D-to-0D coupling between the field and the circuit. The number of nonzeros scales as $\mathcal{O}\left(n_{\mathrm{1D}}^3\right)$ where n_{1D} stands for the number of degrees of freedom in one spatial direction. The number of nonzeros in $\widetilde{\mathbf{C}}\mathbf{M}_\nu\mathbf{C}$ and $\mathbf{M}_\sigma$ scales by $\mathcal{O}\left(n_{\mathrm{1D}}^3\right)$ as well, such that the computation time for the application of $\mathbf{Q}_{\mathrm{sol},q}$ is expected to have the same complexity as the one for the application of the field model.

A second coupling strategy exploits the non-uniqueness of $\mathbf{A}$ and ϕ and even may consider potentials that are not continuous in parts of Ω [14]. The voltage drop is introduced as a step potential difference at an arbitrary reference cross-section $\Gamma_{\mathrm{sol},q}$

which cuts $\Omega_{\mathrm{sol},q}$ in two parts without touching the electrodes. In the discrete setting, the voltage drop is assigned to the primary edges corresponding to a set of dual facets covering $\Gamma_{\mathrm{sol},q}$. The discrete source-current vector then reads $\widehat{\widehat{\mathbf{j}}}_{\mathrm{s}} = \mathbf{M}_\sigma \tilde{\mathbf{Q}}_{\mathrm{sol},q} u_{\mathrm{sol},q}$ where $\tilde{\mathbf{Q}}_{\mathrm{sol},q}$ contains 0, 1 and -1 indicating the contribution and orientation of primary edges with respect to the reference cross-section $\Gamma_{\mathrm{sol},q}$. In contrast to $\mathbf{Q}_{\mathrm{sol},q}$, the coupling operator $\tilde{\mathbf{Q}}_{\mathrm{sol},q}$ represents a 2D-to-0D field-circuit coupling which has a complexity that only scales by $\mathcal{O}\left(n_{\mathrm{1D}}^2\right)$ and which consequently guarantees the efficiency of the field-circuit coupling scheme.

The total current $i_{\mathrm{sol},q}$ through the massive conductor q is integrated at $\Gamma_{\mathrm{sol},q}$ which, in the discrete setting, boils down to a summation of the currents through the dual facets covering $\Gamma_{\mathrm{sol},q}$:

$$i_{\mathrm{sol},q} = \tilde{G}_{\mathrm{sol},q} u_{\mathrm{sol},q} - \tilde{\mathbf{Q}}_{\mathrm{sol},q} \frac{d\widehat{\mathbf{a}}}{dt} \tag{11}$$

where $\tilde{G}_{\mathrm{sol},q} = \tilde{\mathbf{Q}}_{\mathrm{sol},q}^T \mathbf{M}_\sigma \tilde{\mathbf{Q}}_{\mathrm{sol},q}$ reflects the discrete conductance of the reference cross-section. A field-circuit coupling involving only the massive conductor q excited by a current source then reads

$$\begin{bmatrix} \tilde{\mathbf{C}}\mathbf{M}_\nu\mathbf{C} & -\mathbf{M}_\sigma\tilde{\mathbf{Q}}_{\mathrm{sol},q} \\ \mathbf{0} & \tilde{G}_{\mathrm{sol},q} \end{bmatrix} \begin{bmatrix} \widehat{\mathbf{a}} \\ u_{\mathrm{sol},q} \end{bmatrix} + \begin{bmatrix} \mathbf{M}_\sigma & \mathbf{0} \\ -\tilde{\mathbf{Q}}_{\mathrm{sol},q}^T\mathbf{M}_\sigma & \mathbf{0} \end{bmatrix} \frac{d}{dt} \begin{bmatrix} \widehat{\mathbf{a}} \\ u_{\mathrm{sol},q} \end{bmatrix} = \begin{bmatrix} \mathbf{0} \\ i_{\mathrm{sol},q} \end{bmatrix} \tag{12}$$

which after time discretisation and appropriate scaling of the single circuit equation yields a symmetric, semi-positive-definite system of equations. A symmetric coupling can also be achieved using $\mathbf{Q}_{\mathrm{sol},q}$ instead of $\tilde{\mathbf{Q}}_{\mathrm{sol},q}$ and $G_{\mathrm{sol},q} = \mathbf{Q}_{\mathrm{sol},q}^T \mathbf{M}_\sigma \mathbf{Q}_{\mathrm{sol},q}$ instead of $\tilde{G}_{\mathrm{sol},q}$. In that case, $G_{\mathrm{sol},q}$ is the DC conductance of the massive conductor and the summation by $\mathbf{Q}_{\mathrm{sol},q}^T$ computes the current by averaging the currents evaluated at all possible discrete cross-sections of the massive conductor with the dual grid.

The 3D-to-0D coupling operator $\mathbf{Q}_{\mathrm{sol},q}$ is disadvantageous for reasons of numerical efficiency. In Table 1, the performance of the Conjugate-Orthogonal Conjugate-Gradient (COCG) solver [34], preconditioned by the Symmetric Successive Over-relaxation (SSOR) algorithm is compared for a coupling with $\mathbf{Q}_{\mathrm{sol},q}$ and a coupling with $\tilde{\mathbf{Q}}_{\mathrm{sol},q}$. For both test models, the number of iterations is smaller for the 3D-to-0D coupling than for the 2D-to-0D coupling, indicating the better condition of the system matrix resulting from the tighter 3D-to-0D coupling. This advantage causes the computation time for the small single-phase transformer model to be in favour of the 3D-to-0D coupling. For the larger three-phase transformer model, however, the matrix-vector multiplications by a denser system matrix adversely influences the overall computation time.

The coupling by $\mathbf{Q}_{\mathrm{sol},q}$ splits the current $\widehat{\widehat{\mathbf{j}}}$ in a source-current part $\widehat{\widehat{\mathbf{j}}}_{\mathrm{s}} = \mathbf{M}_\sigma \mathbf{Q}_{\mathrm{sol},q} u_{\mathrm{sol},q}$ and an eddy-current part $\widehat{\widehat{\mathbf{j}}}_{\mathrm{e}} = -\mathbf{M}_\sigma \frac{d}{dt}\widehat{\mathbf{a}}$ that are both free of divergence. The sparser coupling by $\tilde{\mathbf{Q}}_{\mathrm{sol},q}$ is related to a division of the divergence-free current $\widehat{\widehat{\mathbf{j}}}$ into two non-divergence-free parts $\widehat{\widehat{\mathbf{j}}}_{\mathrm{s}} = \mathbf{M}_\sigma \tilde{\mathbf{Q}}_{\mathrm{sol},q} u_{\mathrm{sol},q}$ and $\widehat{\widehat{\mathbf{j}}}_{\mathrm{e}} = -\mathbf{M}_\sigma \frac{d}{dt}\widehat{\mathbf{a}}$ for which a physical interpretation is cumbersome. Special care has to be taken for the algebraic solution of (12). The coupling operator $\tilde{\mathbf{Q}}_{\mathrm{sol},q}$ and hence also the discrete magnetic vector potential $\widehat{\mathbf{a}}$ do not mimic continuous fields. Hence, the system solver may experience increasingly worse condition numbers as the discretisation

Table 1: Iteration counts and solution times for SSOR-COCG applied to a field-circuit coupling with the coupling matrices $\mathbf{Q}_{\mathrm{sol},q}$ and $\mathbf{P}_{\mathrm{str},p}$ or with the coupling matrices $\tilde{\mathbf{Q}}_{\mathrm{sol},q}$ and $\tilde{\mathbf{P}}_{\mathrm{str},p}$.

	coupling matrices	number of iterations	solution time (s)
single-phase	$\tilde{\mathbf{Q}}_{\mathrm{sol},q}$ and $\tilde{\mathbf{P}}_{\mathrm{str},p}$	198	15
transformer	$\mathbf{Q}_{\mathrm{sol},q}$ and $\mathbf{P}_{\mathrm{str},p}$	127	12
three-phase	$\tilde{\mathbf{Q}}_{\mathrm{sol},q}$ and $\tilde{\mathbf{P}}_{\mathrm{str},p}$	756	145
transformer	$\mathbf{Q}_{\mathrm{sol},q}$ and $\mathbf{P}_{\mathrm{str},p}$	465	176

is refined. A stable system solver is mandatory to ensure that the solution for $\widehat{\mathbf{a}}$ alleviates the discontinuity of $\tilde{\mathbf{Q}}_{\mathrm{sol},q}$ such that the non-divergence-free source- and eddy-current densities combine to a physically sound, divergence-free discrete current distribution.
The field-circuit coupling approach can be understood as an *agglomeration* of *local* field quantities into *global* circuit quantities [14]. In the FIT and in other discretisation techniques closely related to differential geometry, this agglomeration is representable by a simple incidence relation [25, 14, 19].

3.2 Stranded-conductor model

When the wire diameter of a coil is significantly smaller than the expected skin depth, is not necessary to resolve each individual wire by the computational grid. Instead, the stranded-conductor model includes the assumption that the current is homogeneously distributed along the cross-section of the coil. The conventional treatment of coils in a 3D field model is to compute the discrete current distribution due to a unit current applied to coil p by a geometric algorithm, yielding the vector field $\mathbf{J}_{\mathrm{unit},p}$. In the FIT case, this continuous current is integrated over the dual facets, whereas in the FE case, edge elements are applied for weighting:

$$\mathbf{P}^{(\mathrm{fit})}_{\mathrm{str},p,i} = \int_{\tilde{S}_i} \mathbf{J}_{\mathrm{unit},p} \cdot \mathrm{d}S \; ; \tag{13}$$

$$\mathbf{P}^{(\mathrm{fe})}_{\mathrm{str},p,i} = \int_{\Omega_{\mathrm{str},p}} \mathbf{J}_{\mathrm{unit},p} \cdot \mathbf{w}_i \mathrm{d}\Omega \; . \tag{14}$$

In both cases, the applied current density reads $\widehat{\mathbf{j}} = \mathbf{P}_{\mathrm{str},p} i_{\mathrm{str},p}$. The coupling operator $\mathbf{P}_{\mathrm{str},p}$ connects all dual facets inside the coil volume $\Omega_{\mathrm{str},p}$ to the circuit and hence, also has the nature of a 3D-to-0D coupling, possibly causing a degeneration of the performance of the coupled simulation. Eddy currents are prohibited by omitting the eddy-current term in the field formulation. The voltage drop along the coil is

$$u_{\mathrm{str},p} = R_{\mathrm{str},p} i_{\mathrm{str},p} + \mathbf{P}^T_{\mathrm{str},p} \frac{d\widehat{\mathbf{a}}}{dt} \tag{15}$$

where $R_{\mathrm{str},p}$ is the DC resistance of the coil and $\mathbf{P}_{\mathrm{str},p}$ averages the voltage drop of all filamentary wires in the coil. The field-circuit coupling of a single coil p excited by a voltage source reads

$$\begin{bmatrix} \widetilde{\mathbf{C}}\mathbf{M}_\nu\mathbf{C} & -\mathbf{P}_{\mathrm{str},p} \\ \mathbf{0} & \tilde{R}_{\mathrm{str},p} \end{bmatrix} \begin{bmatrix} \widehat{\mathbf{a}} \\ i_{\mathrm{str},p} \end{bmatrix} + \begin{bmatrix} \mathbf{0} & \mathbf{0} \\ \mathbf{P}^T_{\mathrm{str},p} & \mathbf{0} \end{bmatrix} \frac{d}{dt} \begin{bmatrix} \widehat{\mathbf{a}} \\ i_{\mathrm{str},p} \end{bmatrix} = \begin{bmatrix} \mathbf{0} \\ u_{\mathrm{str},p} \end{bmatrix} \; . \tag{16}$$

Also for coils, a 2D-to-0D coupling scheme can be developed [17, 14]. The homogeneous current distribution is only applied to the dual facets covering a reference cross-section $\Gamma_{\mathrm{str},p}$, i.e., $\hat{\tilde{\mathbf{j}}} = \tilde{\mathbf{P}}_{\mathrm{str},p} i_{\mathrm{str},p}$ where the dimension-less coupling operator $\tilde{\mathbf{P}}_{\mathrm{str},p}$ contains the relative orientations of the participating dual facets with respect to $\Gamma_{\mathrm{str},p}$. The current distribution is forced to remain homogeneous throughout the entire coil by an anisotropic conductivity matrix added to the magnetoquasistatic field problem. In the FE case, the conductivity matrix reads

$$\mathbf{M}^{\mathrm{fe}}_{\sigma,\mathrm{coil},i,j} = \int_{\Omega_{\mathrm{str},p}} \sigma \left(\mathbf{w}_i \cdot \mathbf{t}_{\mathrm{str},p}\right) \left(\mathbf{w}_j \cdot \mathbf{t}_{\mathrm{str},p}\right) \mathrm{d}\Omega \tag{17}$$

where $\mathbf{t}_{\mathrm{str},p}$ denotes the direction of the wires of coil p. The summation by $\tilde{\mathbf{P}}_{\mathrm{str},p}$ corresponds to an integration of the electric field along a reference layer. $\tilde{R}_{\mathrm{str},p} = \tilde{\mathbf{P}}^T_{\mathrm{str},p} \mathbf{M}^{\dagger}_{\sigma,\mathrm{coil}} \tilde{\mathbf{P}}_{\mathrm{str},p}$ where $\dagger$ denotes a pseudo-inverse carried out for the nonzero parts of $\mathbf{M}_{\sigma,\mathrm{coil}}$ only, represent the resistance of the reference layer. The 2D-to-0D coupling of a stranded-conductor model is found by replacing $\mathbf{P}_{\mathrm{str},p}$ by $\tilde{\mathbf{P}}_{\mathrm{str},p}$ and $R_{\mathrm{str},p}$ by $\tilde{R}_{\mathrm{str},p}$ in (16). The same remarks concerning the algebraic solver apply as for the solid-conductor case.

3.3 Specialised conductor models

Massive conductors and wire coils are adequately modelled by solid- and stranded-conductor models respectively. In engineering practice, however, more complicated coils and winding schemes exist. Particular distribution transformers and inductors contain foil windings, which are constructed by rolling up sheets of conductive material. The current through the sheet cross-section remains constant. However, a significant redistribution of the current towards the tips of the sheet occurs. In particular devices, the eddy-current effects can also not be neglected in the individual wires of the windings. Especially when then number of turns becomes very large, it is not recommended to resolve the individual sheets or wires by the FE or FIT mesh, even if significant eddy-current effects are expected [9]. The discretisation for the magnetic vector potential should resolve the skin depth but should not necessarily adapt to the size of individual wires. The choice for a particular conductor model is motivated by the ratio of the conductor sizes d_x and d_y and the expected skin depths δ_x and δ_y (Fig. 2). The magnetic flux penetrates a stranded-conductor model because no eddy currents occur (Fig. 3a). For a solid-conductor model, the magnetic flux is expelled in both directions because of eddy-current effects (Fig. 3c), whereas in the foil-conductor case, the magnetic flux is only expelled in the direction towards the tips of the sheets (Fig. 3b).

For foil windings, dedicated foil-conductor models applicable within 2D and 3D FE models have been proposed in [9] and [16]. For windings with a rectangular wire cross-section, a multi-conductor model has been proposed in [10]. These methods avoid the explicit consideration of the separate turns by assuming a smooth variation of the turn voltages over the reference cross-section of the winding. This voltage drop is discretised at an additional mesh defined at the reference cross-section. A weak formulation is applied to force the currents through the turns to be the same at the control volumes corresponding to the turn-voltage discretisation. Such coil models

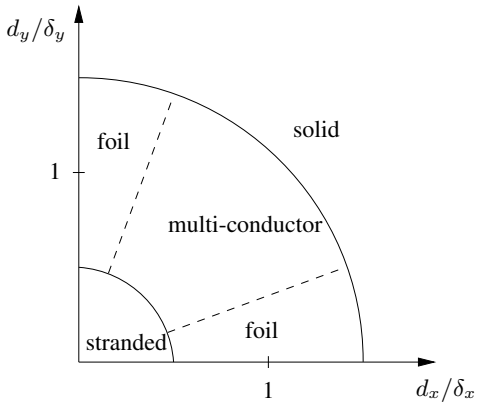

Fig. 2: Application range of the solid-, stranded-, foil- and multi-conductor models.

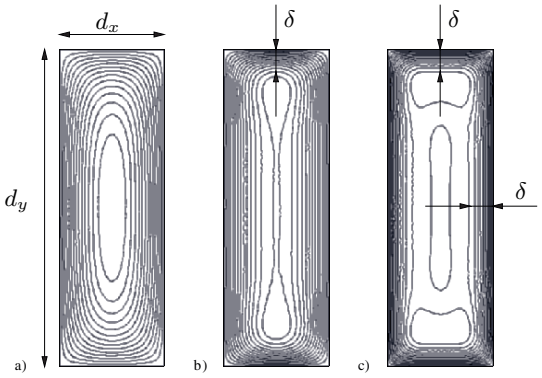

Fig. 3: Magnetic flux lines within (a) a stranded, (b) a foil and (c) a solid conductor of equal size and with the same number of Ampère-turns.

are especially efficient for windings where the spatial scale of the turn-voltage variation and the spatial scale of the eddy-current redistribution is substantially larger than the smallest dimension of the individual wires or sheets. More details about the mathematical formulation of the foil-conductor model can be found in [9] and [16]. The formulation of the wire-conductor case is developed in [10].

4 Field-Circuit Coupling

The relations between the currents and the voltage drops of solid- and stranded-conductor models connected within the circuit are expressed by (11) and (15) respectively. These relation can be interpreted as controlled current and voltage sources [13, 11]. The inversion of the expression is cumbersome because of the presence of the time derivative and especially because of the coupling to the field model. No additional circuit equations are needed if the voltage drops along the massive conductors and the currents through the coils are known on beforehand [23, 33]. If this is not the case, the voltage drops along the massive conductors and the currents

through the stranded conductors should appear as degrees of freedom in the circuit system. A systematic description of the circuit problem accounting for this consists of a division of the circuit into a tree and a co-tree while forcing the solid conductors (together with the voltage sources and the capacitors) and the stranded conductors (together with the current sources and the inductors) to be part of the tree and the co-tree respectively. Here, we assume that such a decomposition is possible. When this is not the case, appropriate mitigation techniques are discussed in [13] and [11]. The fundamental cutset matrix $\mathbf{D}$ and the fundamental loop matrix $\mathbf{B}$ are partitioned with respect to the solid-conductor, capacitor and resistor tree branches by the subscript $\cdot_{\mathrm{two}}$, with respect to the stranded-conductor, inductor and resistor links by the subscript $\cdot_{\mathrm{lno}}$ and with respect to the independent voltage and current sources by the subscripts $\cdot_{\mathrm{twu}}$ and $\cdot_{\mathrm{lni}}$ respectively. The coupling operators are brought together into $\mathbf{Q}_{\mathrm{sol}}$ and $\mathbf{P}_{\mathrm{str}}$, possibly adding zero columns to account for non-coupled circuit branches. The conductances and resistances of the circuit resistors and the coupled solid- and stranded-conductor models are collected in the diagonal matrices $\mathbf{G}_{\mathrm{two}}$ and $\mathbf{R}_{\mathrm{lno}}$. Similarly, the capacitances and inductances of the circuit branches are gathered in $\mathbf{C}_{\mathrm{two}}$ and $\mathbf{L}_{\mathrm{lno}}$ respectively. The voltages and currents of the independent sources are denoted by u_{twu} and i_{lni} respectively. Then, the field-circuit coupling reads

$$\begin{bmatrix} \widetilde{\mathbf{C}}\mathbf{M}_\nu\mathbf{C} & -\mathbf{M}_\sigma\mathbf{Q}_{\mathrm{sol}} & -\mathbf{P}_{\mathrm{str}} \\ \mathbf{0} & \mathbf{G}_{\mathrm{two}} & \mathbf{D}_{\mathrm{two,lno}} \\ \mathbf{0} & \mathbf{B}_{\mathrm{lno,two}} & \mathbf{R}_{\mathrm{lno}} \end{bmatrix} \begin{bmatrix} \widehat{\mathbf{a}} \\ \mathbf{u}_{\mathrm{two}} \\ \mathbf{i}_{\mathrm{lno}} \end{bmatrix} + \begin{bmatrix} \mathbf{M}_\sigma & \mathbf{0} & \mathbf{0} \\ -\mathbf{Q}_{\mathrm{sol}}^T\mathbf{M}_\sigma & \mathbf{C}_{\mathrm{two}} & \mathbf{0} \\ \mathbf{P}_{\mathrm{str}}^T & \mathbf{0} & \mathbf{L}_{\mathrm{lno}} \end{bmatrix} \frac{d}{dt} \begin{bmatrix} \widehat{\mathbf{a}} \\ \mathbf{u}_{\mathrm{two}} \\ \mathbf{i}_{\mathrm{lno}} \end{bmatrix} = \begin{bmatrix} \mathbf{0} \\ -\mathbf{D}_{\mathrm{two,lni}}\mathbf{i}_{\mathrm{lni}} \\ -\mathbf{B}_{\mathrm{lno,twu}}\mathbf{u}_{\mathrm{twu}} \end{bmatrix} . \tag{18}$$

Notice that the circuit description is organised such that no fill-in in the field system part appears.

5 Time Integration

5.1 Singly diagonally implicit Runge-Kutta method

The coupled system of equations, here abbreviated to $\mathbf{K}\mathbf{x}+\mathbf{M}\frac{d}{dt}\mathbf{x} = \mathbf{f}$, is integrated in time by an implicit Runge-Kutta method [24, 28, 6]. The stage vectors $\bar{\mathbf{x}}_i$ and the stage derivatives $\dot{\mathbf{x}}_i$ for n_{stage} stages $i = 1, \ldots, n_{\mathrm{stage}}$ of the algorithm relate the solution $\mathbf{x}_n$ at the old time instant t_n to two solutions $\mathbf{x}_{n+1}$ and $\tilde{\mathbf{x}}_{n+1}$ of different order of approximation at the new time instant $t_{n+1} = t_n + \tau_{n+1}$ by

$$\bar{\mathbf{x}}_i = \mathbf{x}_n + \tau_{n+1} \sum_{j=1}^{n_{\mathrm{stage}}} a_{ij}\dot{\mathbf{x}}_j \ , \quad i = 1, \ldots, n_{\mathrm{stage}} \tag{19}$$

$$\mathbf{x}_{n+1} = \mathbf{x}_n + \tau_{n+1} \sum_{j=1}^{n_{\mathrm{stage}}} b_j\dot{\mathbf{x}}_j \tag{20}$$

$$\tilde{\mathbf{x}}_{n+1} = \mathbf{x}_n + \tau_{n+1} \sum_{j=1}^{n_{\mathrm{stage}}} \tilde{b}_j\dot{\mathbf{x}}_j \ . \tag{21}$$

$1-\sqrt{2}/2$		$1-\sqrt{2}/2$	0	0	0
1		$\sqrt{2}/2$	$1-\sqrt{2}/2$	0	0
$\sqrt{2}/2$		$5-3\sqrt{2}$	$2\sqrt{2}-6$	$1-\sqrt{2}/2$	0
1		$\sqrt{2}/3+1/6$	$\sqrt{2}/6-1/3$	$1/6$	$1-\sqrt{2}/2$
order	3	$\sqrt{2}/3+1/6$	$\sqrt{2}/6-1/3$	$1/6$	$1-\sqrt{2}/2$
order	2	$\sqrt{2}/2$	$1-\sqrt{2}/2$	0	0
order	1	$1/2$	$1/8$	$1/4$	$1/8$

Fig. 4: Butcher table for the applied singly diagonally implicit Runge-Kutta method with four stages, a solution of 3rd order, an embedded solution of 2nd order and an embedded solution of 1st order.

The coefficients a_{ij}, b_j and $\tilde{b}_j$ are collected in a Butcher table [6]. Here, we consider a singly diagonally implicit Runge-Kutta method with four stages, achieving a solution of 3rd order and an embedded solution of 2nd order (SDIRK-3(2)) for which the coefficients are listed in Fig. 4. For each stage i, the system

$$\left(\mathbf{K}+\frac{1}{a_{ii}\tau_{n+1}}\mathbf{M}\right)\bar{\mathbf{x}}_i=\mathbf{f}\left(t_n+c_i\tau_{n+1}\right)+\frac{1}{a_{ii}\tau_{n+1}}\mathbf{M}\mathbf{x}_n+\mathbf{M}\sum_{j=1}^{i-1}\frac{a_{ij}}{a_{ii}}\dot{\mathbf{x}}_j \quad (22)$$

with c_i the coefficients of the left column in Fig. 4, has to be solved. The nonlinearity caused by the dependence of the reluctivity on the magnetic field is resolved by the successive-substitution approach or by the Newton method. The Kirchhoff voltage law (second row in (18)) is scaled by $a_{ii}\tau_{n+1}$ whereas the Kirchhoff current law (3rd row in (18)) is scaled by $-a_{ii}\tau_{n+1}$ in order to achieve a symmetric system of equations. The resulting system is indefinite and is solved by the Minimal Residual method [29] or the Quasi-Minimal Residual method [20] for symmetric, indefinite systems. The system is preconditioned by a block preconditioner using multigrid for the field part and an exact inverse for the circuit part [12]. The 2D examples given in the paper are preconditioned by a multigrid approach developed for field-circuit coupled systems [26].

5.2 Adaptive time-step selection

The difference of both solutions $\mathbf{y}=\mathbf{x}_{n+1}-\tilde{\mathbf{x}}_{n+1}$ is used to control the error of the time-integration process [8, 4]. The error, measured in the norm

$$\|\mathbf{y}\|_{\mathrm{err}}=\sqrt{\sum_j\left(\frac{\mathbf{y}_j}{|\mathbf{x}_{n+1,j}|+\delta_{\mathrm{abs}}}\right)^2} \quad (23)$$

where δ_{abs} is an absolute tolerance, is compared to a user-defined error tolerance ϵ_{tol} multiplied by an acceleration factor μ, typically set slightly larger than 1. If $\|\mathbf{y}\|_{\mathrm{err}}>\mu\epsilon_{\mathrm{tol}}$, the last time step is rejected, otherwise the time step is accepted. The last time step is repeated or a new time step is computed with the time-step length

$$\tau_{n+2}=\rho_{\mathrm{safety}}\left(\frac{\epsilon_{\mathrm{tol}}}{\|\mathbf{y}\|_{\mathrm{err}}}\right)^{1/(\tilde{p}+1)}\tau_{n+1} \quad (24)$$

where $\tilde{p}$ is the order of the embedded solution and ρ_{safety} is a safety factor, typically set to 0.9 [22].

5.3 Sinusoidal dynamics

Many electrotechnical devices are excited by sinusoidal voltages and currents. For that case, a bad performance of the above described error-controlled adaptive time-stepping scheme was observed [5]. This phenomenon is explained by the fact that every second term of the Taylor series expansion of harmonic functions vanishes at particular time instants. Then, the difference between the 3rd order accurate solution and the 2nd order accurate embedded solution is negligible which motivates the time integrator to put very large time steps. A possible alleviation of this problem consists of using an embedded solution that differs by two orders of approximation, e.g., an SDIRK-3(1) method (Fig. 4).

5.4 Time-integration over discontinuities

When field effects due to the switching of power electronic components are considered, the switching events have to be considered by the time integrator [1, 31, 15]. A next time step is computed under the assumption that no switching events occur [2]. Afterwards, a possible event is detected by a sign checking procedure in the case of a θ-type time integrator [30, 18] or by evaluating Sturm sequences in the case of a higher-order time integrator [32, 3]. The time step is reduced to the instant of switching. At this time instant, the field and circuit solutions are determined relying upon the dense output capabilities of the implicit Runge-Kutta method [6]. When due to the switching events, capacitors are short-circuited or inductive chains are opened, a direct redistribution of charge and flux, respectively, is carried out. It also makes sense to carry out direct redistributions in all capacitive loops and all inductive cutsets where the associate time constants are significantly smaller than the time constants of the field problem. Such strategy avoids irrelevant time steps to be carried out for the entire field-circuit coupled system. Another possibility would include the use of a multi-rate time stepping scheme [21], e.g., performing additional small time steps for the circuit, especially when a switching event has occurred. After the computation of consistent initial conditions, the time-integration procedure is restarted with a changed circuit [27]. In our implementation, we favour to change the topology of the circuit, and by that, also the structure and possibly also the size of the system matrix, instead of the approach where switches are modelled by highly nonlinear resistors, causing bad condition numbers of the systems of equations [18, 31].

6 Examples

The first example is a single-phase machine with a start/run capacitor (Fig. 5). Its 2D cross-section is discretised by a finite-element method, resolves local saturation and eddy-current effects by adaptive mesh refinement and models rotor motion by a sliding-surface technique. By transient simulation, the currents through the main and auxiliary windings at start-up are computed.

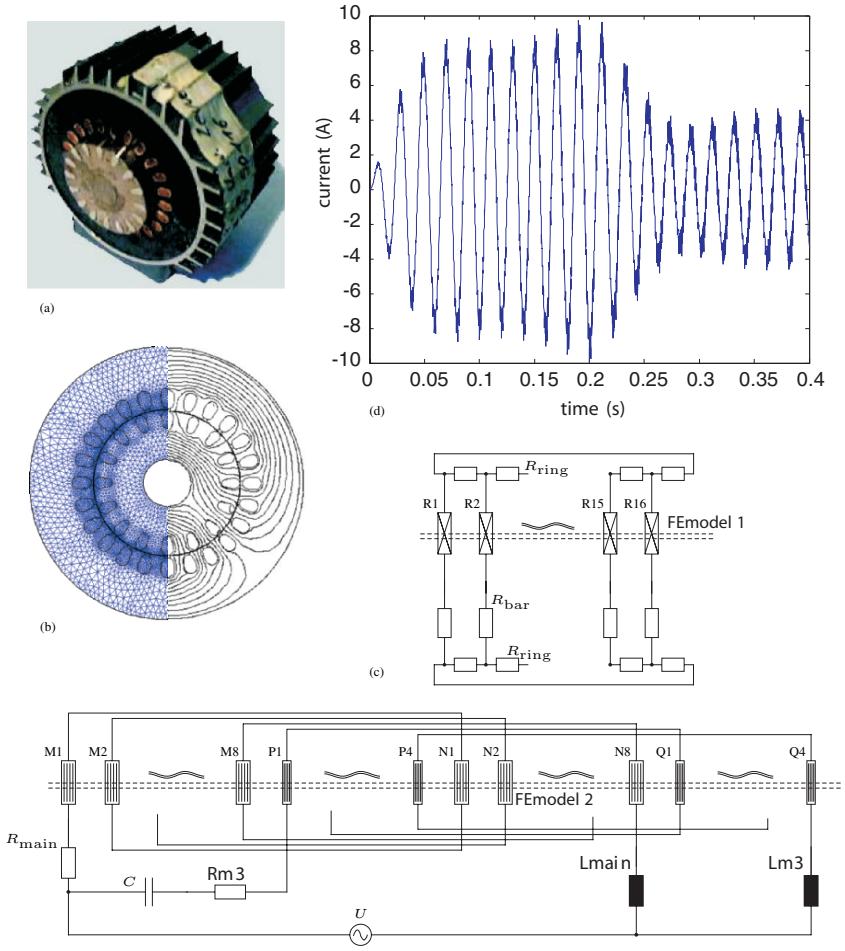

Fig. 5: Capacitor motor: (a) photograph; (b) finite-element mesh and magnetic flux lines at no-load operation; (c) external circuit with the applied sinusoidal voltage U, the capacitance C, the resistances R_{main} and R_{aux} and inductances L_{main} and L_{aux} modelling the end winding parts and the resistances R_{bar} and R_{ring} modelling the rotor ring and rotor-bar parts outside the finite-element model; (d) current through the main stator winding during start-up.

The second example is a three-phase transformer of which the primary side is connected to the grid and the second side is connected to a diode rectifier with an inductive load (Fig. 6). The detection and treatment of switching instants is carried out by a modified SDIRK-3(2) time integrator. Here, the capability of simulating immediate flux redistribution is exploited (Fig. 7).

7 Conclusions

Field-circuit coupling is extremely important to obtain reliable simulation results for electrical devices in an efficient way. The coupling between the degrees of freedom of the field formulation and the ones of the circuit formulation has to be designed such that no computational bottleneck arises, e.g., by too dense algebraic coupling

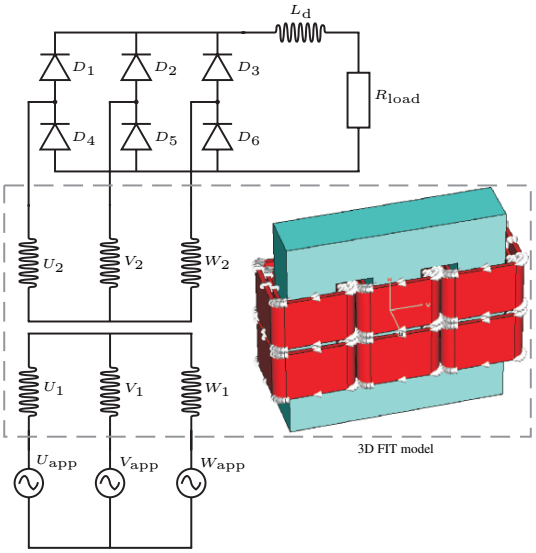

Fig. 6: 3D finite-integration model of a three-phase transformer connected to an external electric circuit for the power grid, diode rectifier and inductive load.

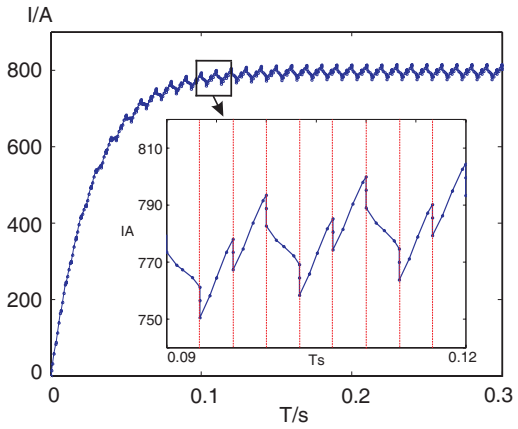

Fig. 7: Current through the first coil at the high-voltage side of the three-phase transformer.

matrices. Besides the traditional solid- and stranded-conductor models commonly applied for massive bars and wire coils within the field model, specialised conductor models exist and should be applied, e.g. for foil windings. An arbitrary connection of conductor models within an external circuit possibly incorporating switches is possible. The time integrator applied to the field-circuit coupled problem should detect and localise the switching events. The time step is restricted to this time instant. Fast dynamics due to (almost) short-circuited capacitors and opened inductive chains are resolved without superfluously evaluating the expensive field problem.

Acknowledgment

The work of H. De Gersem is supported by the Gesellschaft für Schwerionenforschung, Darmstadt, Germany. G. Benderskaya is supported by the Computational Engineering Research Center at the Technische Universität Darmstadt.

References

1. A. Arkkio. Finite element analysis of cage induction motors fed by static frequency converters. *IEEE Trans. Magn.*, 26(2):551–554, March 1990.
2. P. Barton and C. Pantelides. Modeling of combined discrete/continuous processes. *AIChE J.*, 40(6):966–979, 1994.
3. G. Benderskaya, M. Clemens, H. De Gersem, and T. Weiland. Embedded Runge-Kutta methods for field-circuit coupled problems with switching elements. *IEEE Trans. Magn.*, 41(5):1612–1615, May 2005.
4. G. Benderskaya, H. De Gersem, M. Clemens, and T. Weiland. Transient field-circuit coupled formulation based on the finite integration technique and a mixed circuit formulation. *COMPEL*, 23(4):968–976, 2004.
5. G. Benderskaya, H. De Gersem, and T. Weiland. Adaptive time integration for electromagnetic models with sinusoidal excitation. In *Proc. Int. Workshop Elec. Magn.*, pages 107–108, Aussois, France, June 2006.
6. F. Cameron. *Low-order Runge-Kutta methods for differential-algebraic equations*. PhD thesis, Tampere University of Technology, Tampere, Finland, 1999.
7. M. Clemens and T. Weiland. Transient eddy-current calculation with the FI-method. *IEEE Trans. Magn.*, 35(3):1163–1166, May 1999.
8. M. Clemens, M. Wilke, and T. Weiland. 3D transient eddy-current simulations using FI^{2}TD with variable time step size selection schemes. *IEEE Trans. Magn.*, 38(2): 605–608, March 2002.
9. H. De Gersem and K. Hameyer. A finite element model for foil winding simulation. *IEEE Trans. Magn.*, 37(5):3427–3432, September 2001.
10. H. De Gersem and K. Hameyer. A multi-conductor model for finite element eddy current simulation. *IEEE Trans. Magn.*, 38(2):533–536, March 2002.
11. H. De Gersem, K. Hameyer, and T. Weiland. Field-circuit coupled models in electromagnetic simulation. *J. Comput. Appl. Math.*, 168(1-2):125–133, July 2004.
12. H. De Gersem, R. Mertens, D. Lahaye, S. Vandewalle, and K. Hameyer. Solution strategies for transient, field-circuit coupled systems. *IEEE Trans. Magn.*, 36(4):1531–1534, July 2000.
13. H. De Gersem, R. Mertens, U. Pahner, R. Belmans, and K. Hameyer. A topological method used for field-circuit coupling. *IEEE Trans. Magn.*, 34(5):3190–3193, September 1998.
14. H. De Gersem and T. Weiland. Field-circuit coupling for time-harmonic models discretized by the finite integration technique. *IEEE Trans. Magn.*, 40(2):1334–1337, March 2004.
15. A. Demenko. Time-stepping FE analysis of electric motor drives with semiconductor convertors. *IEEE Trans. Magn.*, 30(5):3264–3267, September 1994.
16. P. Dular and C. Geuzaine. Spatially dependent global quantities associated with 2D and 3D magnetic vector potential formulations for foil winding modeling. *IEEE Trans. Magn.*, 38(2):633–636, March 2002.
17. P. Dular and J. Gyselinck. Modeling of 3-D stranded inductors with the magnetic vector potential formulation and spatially dependent turn voltages of reduced support. *IEEE Trans. Magn.*, 40(2):1298–1301, March 2004.
18. P. Dular and P. Kuo-Peng. An efficient time discretization procedure for finite element-electronic circuit equation coupling. *COMPEL*, 21(2):274285, 2002.

19. P. Dular, R. Specogna, and F. Trevisan. Coupling between circuits and A-χ discrete geometric approach. *IEEE Trans. Magn.*, 42(4):1043–1046, April 2006.
20. R. Freund and N.M. Nachtigal. A new Krylov-subspace method for symmetric indefinite linear systems. In W.F. Ames, editor, *Proceedings of the 14th IMACS World Congress on Computational and Applied Mathematics*, pages 1253–1256, 1994.
21. M. Günther and P. Rentrop. Multirate ROW methods and latency of electrical circuits. *Appl. Numer. Math*, 13:83–102, 1993.
22. K. Gustafsson. Control-theoretic techniques for stepsize selection in implicit Runge-Kutta methods. *ACM Trans. Math. Software*, 20(4):496–517, December 1994.
23. J. Gyselinck and J. Melkebeek. Numerical methods for time stepping coupled field-circuit systems. In *Proceedings of the International Conference on Modelling and Simulation of Electric Machines, Converters and Systems (ELECTRIMACS 96)*, volume 1, pages 227–234, Saint-Nazaire, France, September 1996.
24. E. Hairer and G. Wanner. *Solving ordinary differential equations, stiff and differential-algebraic problems*. Springer-Verlag, Berlin, 2 edition, 1996.
25. L. Kettunen. Fields and circuits in computational electromagnetism. *IEEE Trans. Magn.*, 37(5):3393–3396, September 2001.
26. D. Lahaye, K. Hameyer, and S. Vandewalle. An algebraic multilevel preconditioner for field-circuit coupled problems. *IEEE Trans. Magn.*, 38(2):413–416, March 2002.
27. G. Mao and L.R. Petzold. Efficient integration over discontinuities for differential-algebraic systems. *Comput. Math. Appl.*, 43:65–79, 2002.
28. A. Nicolet and F. Delincé. Implicit Runge-Kutta methods for transient magnetic field computations. *IEEE Trans. Magn.*, 32(3):1405–1408, May 1996.
29. C.C. Paige and M.A. Saunders. Solution of sparse indefinite systems of linear equations. *SIAM J. Numer. Anal.*, 12(4):617–629, 1975.
30. A.J. Preston and M. Berzins. Algorithms for the location of discontinuities in dynamic simulation problems. *Comput. Chem. Eng.*, 15(10):701–713, 1991.
31. N. Sadowski, B. Carly, Y. Lefevre, M. Lajoie-Mazenc, and S. Astier. Finite element simulation of electrical motors fed by current inverters. *IEEE Trans. Magn.*, 29(2):1683–1688, March 1993.
32. L.F. Shampine, I. Gladwell, and R.W. Brankin. Reliable solution of special event localisation problems for ODEs. *ACM Trans. Math. Soft.*, 17(1):11–25, March 1991.
33. I.A. Tsukerman, A. Konrad, G. Meunier, and J.C. Sabonnadière. Coupled field-circuit problems: trends and accomplishments. *IEEE Trans. Magn.*, 29(2):1701–1704, March 1993.
34. H.A. Van der Vorst and J.B.M. Melissen. A Petrov-Galerkin type method for solving $Ax = b$, where A is symmetric complex. *IEEE Trans. Magn.*, 26(2):706–708, March 1990.
35. T. Weiland. A discretisation method for the solution of Maxwell's equations for six-component fields. *Electr. Commun. AE*, 31:116–120, 1977.
36. T. Weiland. Time domain electromagnetic field computation with finite difference methods. *Int. J. Num. Mod.*, 9(4):295–319, July-August 1996.